PCCP

PAPER

View Article Online
View Journal | View Issue

Cite this: *Phys. Chem. Chem. Phys.*, 2019, **21**, 12667

Anomalous kinetics of the reaction between OH and HO_2 on an accurate triplet state potential energy surface

Yang Liu,[a] Mengna Bai,[a] Hongwei Song, *[b] Daiqian Xie *[c] and Jun Li *[a]

Received 20th March 2019,
Accepted 20th May 2019

DOI: 10.1039/c9cp01553a

rsc.li/pccp

The reaction OH + HO_2 → H_2O + O_2 is of great significance in interstellar media, the atmosphere, and combustion. In addition, it presents a prototypical reaction between two non-atom radical species. However, the temperature dependence of its rate coefficients has been debated for several decades. In this work, the rate coefficients are revisited by the quasi-classical trajectory (QCT) approach. To this end, a globally accurate full-dimensional potential energy surface of the ground triplet state for the title reaction is constructed using the permutation invariant polynomial-neural network (PIP-NN) method based on 108 000 points calculated at the level of CCSD(T)-F12a/AVTZ, in which particular attention is paid to the initial guess in the preceding Hartree–Fock procedure to obtain reliable *ab initio* energies. The QCT rate coefficients are compared to available experimental and theoretical results. It has been found that not only the trend, but also the magnitude, *i.e.* the large negative temperature dependence at low temperatures, and slightly positive temperature dependence at high temperatures, are consistent with some experiments.

I. Introduction

The reaction OH + HO_2 → H_2O + O_2 (R1) is a chain termination reaction. It plays an important role in astrochemistry and combustion chemistry. On one hand, not only the reaction itself, but also the involved species, reactants or products, are of great significance in interstellar, atmospheric, and combustion environments.[1] In the upper atmosphere, R1 is a dominant reaction pathway in the removal of OH and HO_2 radicals, which are involved in several catalytic cycles related to other radicals, O, O_3, ClO_x, and NO_x, that play a significant role in the atmosphere.[2–10] On the other hand, this reaction is also an important process in combustion chemistry. Under lean combustion conditions, it is a major consumption process of HO_2 and responsible for the depletion of both radicals in burnt gases.[11–13] In addition, R1 is also helpful in establishing the mechanism and kinetics for peroxy–peroxy radical reactions, RO_2 + $R'O_2$, which are important in the combustion and atmospheric oxidation of hydrocarbons.[14] Last but not the least, it presents a long-standing challenging problem to the experimentalist, *i.e.* how to accurately measure its rate coefficients. The difficulty in measuring the rate is related to several factors, such as the radical–radical nature of the reaction, the problem of monitoring the radical concentrations (especially HO_2), and the possible complicated side reactions or self-reactions.[15,16] The reaction also provides a serious test for the application of reaction rate theory to elementary radical reactions due to its possible pressure dependence, anomalous temperature dependence, and large rate coefficients. Due to its unique position in the study of radical–radical kinetics, R1 has been referred to as "the Holy Grail Reaction" by Fred Kaufman.[17] Although a large number of experimental and a few theoretical studies have been devoted to this reaction,[13,16,18–20] its thermal rate coefficients are quite scattered with large uncertainty, bringing about significant errors in interstellar, combustion and atmospheric modeling.[16,19,20]

In earlier studies, R1 was assumed to be pressure dependent, which can be related to the complex-forming mechanism, through the intermediate complex HOOOH, namely, OH + HO_2 ↔ HOOOH* → H_2O + O_2.[4,6,15,21] However, later measurements concluded that its rate coefficients exhibit little or no pressure dependence,[5,17,22,23] indicating that R1 takes place mainly *via* a direct abstraction mechanism. In other words, the active HOOOH complex neither dissociates to H_2O + O_2 nor is stabilized by collision.[5,17,21,22] This explanation was verified further by various theoretical investigations.[14,20,24–26] Indeed, pioneering

[a] *School of Chemistry and Chemical Engineering, Chongqing University, Chongqing 401331, China. E-mail: jli15@cqu.edu.cn*
[b] *State Key Laboratory of Magnetic Resonance and Atomic and Molecular Physics, Wuhan Institute of Physics and Mathematics, Chinese Academy of Sciences, Wuhan 430071, China. E-mail: hwsong@wipm.ac.cn*
[c] *Institute of Theoretical and Computational Chemistry, Key Laboratory of Mesoscopic Chemistry, School of Chemistry and Chemical Engineering, Nanjing University, Nanjing, 210093, China. E-mail: dqxie@nju.edu.cn*

theoretical calculations have argued that the recombination channel to form HOOOH is irrelevant,[23] and R1 takes place primarily on the triplet potential energy surface (PES), while the channel to form H_2O and singlet oxygen on the singlet PES can be ignored.[14,23–25,27]

As mentioned above, although there have been numerous experimental measurements, the temperature dependence of the rate coefficients (denoted as k_1) of R1 remained inconclusive. At room temperature around 288–308 K, the observed rate coefficients ranged from 5.2 to 20.0 $\times$ 10^{-11} cm^3 molecule^{-1} s^{-1}.[2,4–7,15,17,21,28–37] Based on 17 sets of experiments at 252–420 K, Sridharan *et al.* showed a negative temperature dependence for k_1 = (1.7 $\pm$ 1.5) $\times$ 10^{-11} exp[(416 $\pm$ 86)/T] or 7.2 $\times$ 10^{-11}(T/296)$^{-n}$ cm^3 molecule^{-1} s^{-1} with n = 1.30 $\pm$ 0.13.[38] Keyser gave k_1 = (4.8 $\pm$ 0.8) $\times$ 10^{-11} exp[(250 $\pm$ 50)/T] cm^3 molecule^{-1} s^{-1} for 254–382 K.[22] At 1400–1800 K, k_1 was estimated to be about 8.3 $\times$ 10^{-11} cm^3 molecule^{-1} s^{-1} in methane–oxygen flames.[11] Goodings and Hayhurst reported k_1 = (1.0 $\pm$ 0.5) $\times$ 10^{-10} cm^3 molecule^{-1} s^{-1} for 1810–2550 K.[39] At 1100 K, Hippler *et al.* obtained 5.0 $\times$ 10^{-11} cm^3 molecule^{-1} s^{-1},[40] or 3.32 $\times$ 10^{-11} cm^3 molecule^{-1} s^{-1} for 950–1250 K,[41] which was fit to 1.66 $\times$ 10^{-11} + 9.6 $\times$ 10^{-11} exp[−2000/T] cm^3 molecule^{-1} s^{-1}.[42] Later, Hippler *et al.* got k_1 at 930–1680 K, and found a minimum at 1250 K.[43] Srinivasan *et al.* estimated k_1 = (4 $\pm$ 3) $\times$ 10^{-11} cm^3 molecule^{-1} s^{-1} for 1200–1700 K.[18] Recently, Hong *et al.* obtained (5.48 $\pm$ 1.49) $\times$ 10^{-11} cm^3 molecule^{-1} s^{-1} for even higher temperatures 1600–2200 K.[13] Within the temperature range 250–2500 K, Hong *et al.* derived k_1 = 1.16 $\times$ 10^{-11} exp[550/T] + 7.47 $\times$ 10^{-10} exp[−5500/T] cm^3 molecule^{-1} s^{-1}.[19]

A few theoretical investigations on R1 have been reported to provide insight into both its reaction mechanism and kinetics. Mozurkewich performed Rice–Ramsperger–Kaassel–Marcus (RRKM) calculations on R1, and both the magnitude and the negative temperature dependence of k_1 are consistent with experiment over the range of 250–420 K.[8] Toohey and Anderson determined a classical barrier height of 2.5 kcal mol^{-1} at the Møller–Plesset perturbation theory level, but proposed a barrierless minimum energy path to explain the large and negative temperature dependence of k_1.[27] Jackels and Phillips carried out a theoretical study to identify the pre-reaction complex, which is 4.7 kcal mol^{-1} more stable than the reactant asymptote using the configuration interaction with all single and double substitutions (CISD) method.[44] Gonzalez *et al.* computed the rate coefficients of R1 in the singlet and triplet state using Møller–Plesset perturbation theory, and concluded that the reaction takes place only on the triplet state PES, due to its submerged barrier.[14,24] The calculated rate coefficients were larger than experiment values with slight negative temperature dependence over 200–2000 K.[24] In 2013, Burke *et al.* employed a multi-scale modeling approach to determine the temperature dependence of k_1. A quantitative explanation for the apparent anomalous temperature dependence, *i.e.* k_1 = 1.93 $\times$ $10^{20}T^{-2.49}$ exp[−294/T] + 1.21 $\times$ $10^{9}T^{1.24}$ exp[658/T] cm^3 molecule^{-1} s^{-1} for 200–3000 K, was provided according to high level *ab initio* calculations and transition state theory. It was found k_1 does have a minimum at 1125 K, however, the temperature dependence is substantially less profound than previously suggested.[16] In the same year, Zhang *et al.* investigated R1 at the CCSD(T)/AVTZ//CCSD/6-311G(d,p) level, and the calculated rate coefficients from transition state theory are smaller than experiment at 298 K.[25] In 2018, Zhang *et al.* revisited R1 at the CCSD(T)/AVTZ//M06-2X/AVTZ level, and the computed rate coefficients are in good agreement with experiment at 298 K.[26]

All the mentioned investigations above provide meaningful information regarding the mechanism and kinetics of the OH + HO_2 reaction. However, the temperature dependence of its rate coefficients has been a persistent source of confusion and debate. In this work, the kinetics of R1 was revisited by advanced theoretical calculations. Specifically, a full dimensional global triplet state PES, which has been found to dominate for the OH + HO_2 reaction, was developed based on 108 000 *ab initio* points calculated at the explicitly correlated coupled cluster single, double, and perturbative triple level with the augmented correlation corrected valence triple-zeta basis set (CCSD(T)-F12a/AVTZ).[45,46] Then these *ab initio* points were fitted to a permutation invariant polynomial-neural network (PIP-NN)[47–49] form with high fidelity. Thermal rate coefficients were then determined on the newly fitted PES using the quasi-classical trajectory (QCT) method. The remainder of the work is organized as follows. The next section (Section II) details the *ab initio* calculations, the PES fitting, and QCT calculation details. Section III presents and discusses the results. A summary and conclusions are given in Section IV.

II. Theory

II-A. *Ab initio* calculations

As has been discussed above, the title reaction occurs exclusively on the ground triplet state PES, even at high temperatures. The geometries of all stationary points, as shown in Fig. 1, were optimized at the explicitly correlated coupled cluster singles, doubles, and perturbative triples level[45,46] associated with the augmented correlation corrected valence double

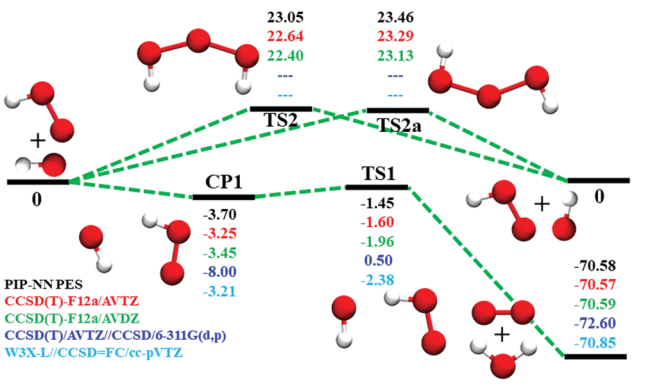

Fig. 1 Schematic illustration of the energetics for the reaction OH + HO_2 on the lowest triplet state PES. All energies are in kcal mol^{-1} and relative to the OH + HO_2 asymptote at various levels: PIP-NN PES, CCSD(T)-F12a/AVTZ, CCSD(T)-F12a/AVDZ, CCSD(T)/AVTZ//CCSD/6-311G(d,p),[25] and W3X-L//CCSD/VTZ,[20] from top to bottom.

or triple-zeta basis set (CCSD(T)-F12a/AVnZ, n = D, T).[45,46] It is well known that CCSD(T)-F12a converges faster with respect to the size of the basis set[45,46] than the standard CCSD(T) calculations. Indeed, CCSD(T)-F12a/AVTZ has been widely used in developing PESs of many reactive and non-reactive systems.[49–52] For both the hydrogen and oxygen atoms, the basis sets are augmented by one more diffuse function for each function type. The default threshold 10^{-6} a.u. was used for the energy convergence in the Hartree–Fock and CCSD(T) calculations. The inner orbitals of the three oxygen atoms were kept frozen in the CCSD(T) calculations. All *ab initio* calculations were carried out using the MOLPRO 2015.1 program package in the current work.[53]

It is emphasized that the title system is multi-reference in nature. As plotted in Fig. 2(a), the calculations at the state averaged full valence complete active space self-consistent field (SA-CASSCF) level, namely 20 electrons in 14 active orbitals (20e, 14o), associated with the VDZ basis set show that the electronic structure varies significantly along the reaction *via* the transition state TS1. In the entrance channel, two singlet and two triplet states are nearly degenerate. In the regions near the transition state TS1, the energy differences between these states start to increase. In the product asymptote, the ground state is a triplet corresponding to $H_2O + O_2$ ($^3\Sigma_g^-$) and other states are much higher. Since we aim to develop a full dimensional PES, all dynamically accessible regions, even far from equilibrium, are required. Indeed, some high-energy regions are necessary to be included for future quantum dynamical calculations. Therefore, it is very hard to select a subset from the complete active space for a reliable description of all regions of the title reaction. Unfortunately, the SA-CASSCF(20e, 14o)/VDZ method takes 4 hours using the Intel Xeon CPU E5-2680 v3 @ 2.50 GHz for a single point energy calculation, and it underestimates the reaction energy of the title reaction significantly, −45.3 kcal mol^{-1}, compared to the experimental value −70.96 kcal mol^{-1}. Therefore, it is still challenging, even impractical, to calculate a large number of configurations for R1 at the multi-reference configuration interaction method (MRCI) level with full valence electron correlation. On the other hand, the single-reference method CCSD(T)-F12a/AVTZ is very likely to converge to wrong electronic states, especially in regions where multiple electronic surfaces are close to each other in energy. In order to obtain a reliable and smooth triplet state PES efficiently, for each configuration, three different initial guesses from the neutral, anion, and cation species are used in the spin-restricted Hartree–Fock calculations, respectively. Then the wavefunction with the lowest Hartree–Fock energy for the neutral species from these different initial guesses was used in the consequent CCSD(T)-F12a procedure based on the fact that Hartree–Fock theory complies with the variational principle. As shown in Fig. 2(b), the CCSD(T)-F12a potentials along the reaction coordinate oscillate abnormally with the initial spin-restricted Hartree–Fock guess from its corresponding neutral, cation, or anion species. If the wavefunction with the lowest Hartree–Fock energy for the neutral species was used in the CCSD(T)-F12a procedure, the potential becomes reasonably smooth. Therefore, this method was chosen as an efficient and reliable (see also discussions below) description of the ground triplet state of the title reaction. For each single point energy calculation with four cores, it takes about 0.5–1.5 hours using the Intel Xeon CPU E5-2680 v3 @ 2.50 GHz.

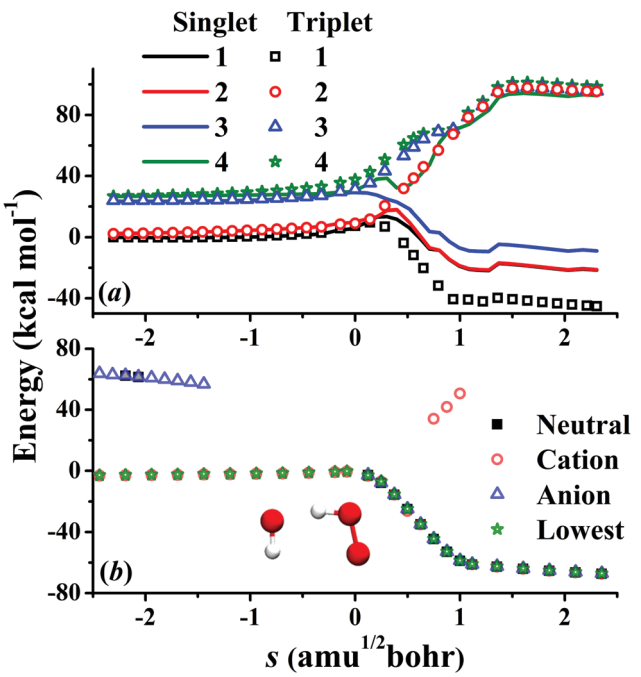

Fig. 2 (a) The SA-CASSCF(20e, 14o)/VDZ calculated energies of the low lying electronic singlet and triplet states as a function of the reaction coordinate of R1. (b) The CCSD(T)-F12a/AVTZ calculated potentials with the initial guess from the corresponding neutral, cation, anion species, and the lowest among them.

II-B. Potential energy surface

The fitting procedure consists of two steps: computing energies of the sampled data points in relevant configurations by the selected *ab initio* method, and fitting them with a specific function. Following our previous strategy,[49,51,52,54–56] possible reaction paths were first surveyed to determine the ranges of configurations and energies. As has been discussed above, two reaction channels were considered with the focus on the lower energy channel to $H_2O + O_2$. Then different grids with appropriate coordinates were used in different regions to sample relevant configurations. For instance, the internal coordinates of HO_2 and OH (the reactant region or the high energy product channel), or of H_2O and O_2 (the low energy product channel), were sampled in dense grids while the coordinates between the two species were sampled with relatively sparse grids. All internal coordinates were sampled with relatively fine grids for the transition state regions. Direct dynamics calculations at a low level of theory, *e.g.* B3LYP/6-31+G(d), were performed to sample points around reaction paths and to determine the ranges of the sampling configurations.

Then the energies of the initial set of points were determined at the selected level, CCSD(T)-F12a/AVTZ, and a primitive PES

was obtained by fitting. With various initial conditions, trajectory calculations were carried out on the raw PES to further explore the configuration space and to generate new points. Next is to exclude points that are too close to each other according to the Euclidean distance $\chi(\{r_i\}) = \sqrt{\sum_i^{10} \left|\vec{r}_i - \vec{r}'_i\right|^2} < 0.2$ Å defined in terms of the internuclear distances between two points, $\{\vec{r}_i\}$ and $\{\vec{r}_i'\}$, in the data set. All permutationally equivalent points (3!2! = 12) were included in such screenings. The PES was also examined by checking key properties of the system, such as geometries, frequencies, and energies of the stationary points, as well as the reaction paths. It should be noted that a small number of high energy points are also necessary for subsequent dynamical studies, especially in quantum mechanical calculations, which will be performed in the near future. The procedure mentioned above was repeated, and the PES was improved gradually.

These selected *ab initio* points were fitted to a permutation invariant polynomial-neural network (PIP-NN) form,[47–49]

$$V = b_1^{(3)} + \sum_{k=1}^{K} \left(\omega_{1,k}^{(3)} \cdot f_2 \left(b_k^{(2)} + \sum_{j=1}^{J} \left(\omega_{k,j}^{(2)} \cdot f_1 \left(b_j^{(1)} + \sum_{i=1}^{I} \omega_{j,i}^{(1)} \cdot G_i \right) \right) \right) \right) \quad (1)$$

where I is the number of PIPs, G_i, of the input layer;[57,58] J and K denote the numbers of the neurons of the two hidden layers, respectively; f_i (i = 1, 2) are the transfer (hyperbolic tangent) functions for the two hidden layers; $\omega_{j,i}^{(l)}$ are weights that connect the ith neuron of the $(l-1)$th layer and the jth neuron of the lth layer; and $b_j^{(l)}$ are biases of the jth neurons of the lth layer. Fitting parameters ω and b were optimized by non-linear least squares fitting of NN with the root mean square error (RMSE) as the performance function: $\mathrm{RMSE} = \sqrt{\sum_{i=1}^{N_{\mathrm{data}}} \left(E_{\mathrm{output}}^i - E_{\mathrm{target}}^i\right)^2 \Big/ N_{\mathrm{data}}}$. The input layer of the NN consists of low-order PIPs, namely, symmetrized monomials of Morse-like variables of internuclear distances, $\mathbf{G} = \hat{S} \prod_{i<j}^{N} p_{ij}^{l_{ij}}$, $p_{ij} = \exp(-\lambda r_{ij})$ (λ = 1.0 Å^{-1}, i, j = 1–5 and $i \neq j$), and $\hat{S}$ the symmetrization operator which explicitly accounts for the invariance with respect to the permutation of the two hydrogen (2!) atoms or of the three oxygen atoms (3!) in the system.[57–59] In this work, the maximum order of the input polynomial is 4, resulting in 138 PIPs. To avoid overfitting, the data were divided randomly into three parts, *i.e.*, the training (90%), validation (5%), and test (5%) sets for each NN fitting. In addition, the "early stop" method[60] was used, in which the training was ceased when the errors of the validating set start to increase. To further circumvent false extrapolation due to edge points in the randomly selected validation and test sets, only fits with similar RMSEs for all three sets were accepted. In addition, the maximum deviation was considered for choosing the final PIP-NN PES. Several different NN architectures with two hidden layers were tested. For each architecture, 100–200 different NN training calculations (different initial fitting parameters, and different training, validation, and test sets) were performed due to the non-linear fitting nature of the NN.

II-C. Quasi-classical trajectory calculations

With the newly fitted PIP-NN PES, the rate coefficients at temperatures of 100, 200, 300, 500, 1000, 2000, and 3000 K were calculated using the QCT approach as implemented in the VENUS chemical dynamics program,[61] according to the following formula:

$$k = f \times \sqrt{\frac{8k_{\mathrm{B}}T}{\pi\mu_{\mathrm{R}}}} \times \pi {b_{\max}}^2 \times \frac{N_{\mathrm{r}}}{N_{\mathrm{total}}} \quad (2)$$

where k_{B} and μ_{R} are the Boltzmann constant and reactant reduced mass, respectively, and f the electronic factor,[24]

$$f = \frac{3}{2(2 + 2\exp(-201.4/T))} \quad (3)$$

The translational, vibrational, and rotational degrees of freedom of the reactants were sampled at the specified temperature with the Boltzmann distribution. At each temperature, its maximal impact parameter ($b_{\max}$) was determined using small batches of trajectories with trial values. The trajectories were initiated at a separation of 12.0 Å and terminated when the products or reactants were separated by 12.0 Å. Other parameters including the relative spatial orientation of the initial reactants, vibrational phases, and the impact parameter, were determined according to the Monte Carlo approach as implemented in VENUS.[61] The propagation time step was selected to be 0.05 fs, and the gradient of the PES with respect to atomic coordinates was calculated numerically. The combined fourth-order Runge–Kutta and sixth-order Adams–Moulton algorithms were used for the integration of the trajectories.[61] Almost all trajectories conserved energy within a chosen criterion (10^{-4} kcal mol^{-1}). At each temperature, 2.0×10^4 trajectories were launched to make the statistical error less than 5.0%.

III. Results

III-A. *Ab initio* calculations

Fig. 1 illustrates the reaction pathways, and the corresponding optimized geometries of the stationary points are presented in Fig. 3. The energies and the harmonic frequencies are listed in Table 1. Note that all the energies are relative to that of the reactant asymptote (without the spin–orbital splitting of OH, which can lower the reactant asymptote by 0.20 kcal mol^{-1}) if not specified. Some recent high level theoretical results are also included for comparison.[20,25] Generally, the results at these levels are consistent with each other. However, apparent deviations do exist for the loose species CP1 and TS1, as discussed below.

Starting from the reactants OH + HO_2, there exist two possible reaction channels. One is to form HO_2 + OH *via* TS2 or TS2a, whose barrier heights are *ca.* 23 kcal mol^{-1}. TS2 and

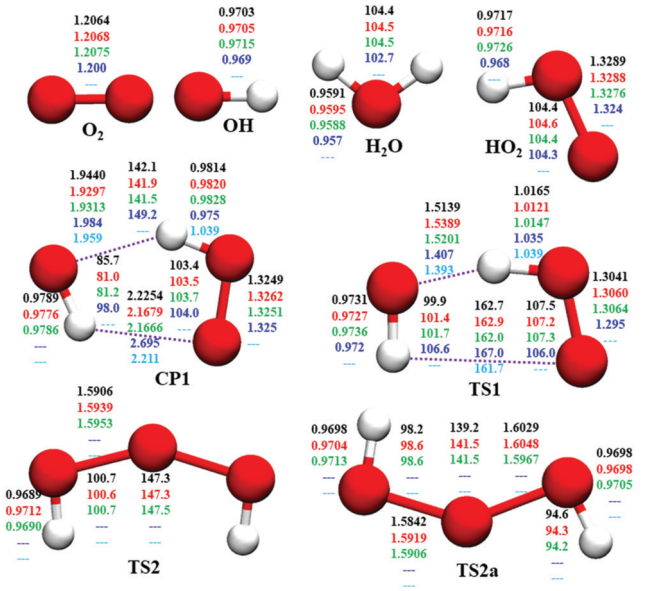

Fig. 3 Comparison of geometries in internal coordinates (distances in Å and angles in degrees) for the stationary points. The values correspond to PIP-NN PES, CCSD(T)-F12a/AVTZ, CCSD(T)-F12a/AVDZ, CCSD/6-311G(d,p),[25] and W3X-L//CCSD = FC/cc-pVTZ,[20] from top to bottom.

TS2a are transition states (TSs) for the oxygen abstraction reaction, but with different steric configurations. To the best of our knowledge, these two TSs have never been reported in the literature. Due to its much higher barrier, this channel is negligible even at high temperatures up to 3000 K, and thus not discussed further. The other channel is to form $H_2O + O_2$ *via* the hydrogen abstraction reaction transition state TS1, which is only −1.6 kcal mol^{-1} at the CCSD(T)-F12a/AVTZ level, making this channel dominant in most cases. TS1 has been calculated at various levels of theory,[20,24–27] and the recent high level results are 0.5 kcal mol^{-1} at the CCSD(T)/AVTZ//CCSD/6-311G(d,p) level,[25] −2.4 kcal mol^{-1} at the W3X-L//CCSD/VTZ level,[20] and −2.1 kcal mol^{-1} at the CCSD(T)/AVTZ//M06-2X/AVTZ level.[26] The deviation comes from the different levels used in the geometry optimization. As shown in Fig. 3, although most coordinates of TS1 from different levels of theory are consistent with each other, the forming bond distance HO$\cdots$HO$_2$ ranges from 1.39 to 1.54 Å. Besides, as shown in Table 1, the imaginary frequency of TS1 is *i*730 cm^{-1}, significantly different from *i*2105 cm^{-1} calculated at the level of W3X-L//CCSD/VTZ.[20] The deviation of the imaginary frequency indicates the difference in the vicinity of the PES near TS1, which generally dominates the reaction.

As shown in Fig. 1, there exists a hydrogen bonded complex well, CP1, between the two radical reactants OH and HO$_2$. At the CCSD(T)-F12a/AVTZ level, it is −3.3 kcal mol^{-1}, which agrees well with −3.2 kcal mol^{-1} at the W3X-L//CCSD/VTZ level,[20] but deviates significantly from other results, ranging from −4.2 to −9.6 kcal mol^{-1} obtained at various levels of theory.[20,24–27,44,62,63] As seen from Fig. 2, the distance between OH and HO$_2$ is sensitive to the calculation methods.

At the CCSD(T)-F12a/AVTZ level, the reaction is highly exothermic, −70.57 kcal mol^{-1}, consistent with −70.85 kcal mol^{-1} calculated at the W3X-L//CCSD/VTZ level,[20] and both are in excellent agreement with −70.96 ± 0.097 kcal mol^{-1} determined by the Active Thermochemical Tables (ATcT) approach.[64,65] They deviate significantly from −72.6 kcal mol^{-1} at the CCSD(T)/AVTZ//CCSD/6-311G(d,p) level,[25] or −69.6 kcal mol^{-1} at the CCSD(T)/AVTZ//M06-2X/AVTZ level.[26]

III-B. Potential energy surface

A total of *ca.* 108 000 points were calculated by the strategy described above, and employed to fit the PES using the PIP-NN approach. Note that a small percentage of points with T_1 diagnostic values larger than 0.05, suggesting some multi-reference character, were discarded. The final PIP-NN PES consists of 30 neurons in each of the two hidden layers, resulting in 5,131 fitting parameters. The total root mean squared error (RMSE) is 12.6 meV, which is slightly larger than other PIP-NN PESs developed by us, presumably due to possible errors introduced by the single reference *ab initio* calculation.

The energies, geometries, and frequencies of the stationary points on the PIP-NN PES are shown in Fig. 1, 3 and Table 1, compared to those calculated directly at the CCSD(T)-F12a/AVnZ (n = D, T) levels. Generally, the results are in good agreement with those at the target *ab initio* calculation level CCSD(T)-F12a/AVTZ, thanks to the high fidelity of the NN fitting. The *ab initio* energies of the stationary points are reproduced with the largest deviation of 0.3 kcal mol^{-1} for the loose structure CP1. The geometric coordinates of the stationary points are also well reproduced: the deviations for rigid distances and angles are within 0.02 Å and 0.5°, respectively, and become larger for floppy coordinates. The harmonic frequencies, including the imaginary frequencies of the TSs, on the PIP-NN PES agree also well with those calculated by CCSD(T)-F12a/AVTZ.

Fig. 4 presents the contour plot along the two reactive bond distances r_{OH} (HO′H$\cdots$O$_2$) and $r_{O'H}$ (HO′$\cdots$HO$_2$) of the dominant reaction channel to $H_2O + O_2$. As shown in the same figure, the minimum energy path (MEP) on the PIP-NN PES is in good accord with that from the direct *ab initio* calculation at the level of CCSD(T)-F12a/AVTZ. Besides, the sampled points with the two reactive bond distances up to 5 Å are also shown in the same figure. It is clearly seen that the sampled points cover all relevant regions with denser points in the low energy region, in particular, of the entrance channel. In order to clearly visualize the topography of the PES, the three-dimensional plot (with other coordinates relaxed) as a function of the breaking and forming bond lengths is shown in Fig. 5, together with the corresponding two-dimensional contour plot. Along the reaction path, the submerged TS1 and the complex CP1 can be clearly seen. Fig. 6 presents the reactive contour plot along the other minor channel, HOO′ + OH → HO + ′OOH. The corresponding MEP, as shown in the same figure, is well reproduced on the PIP-NN PES as well. In addition, it can be seen that this reaction channel is symmetric. Namely, the reactant side and

Table 1 Comparison of the energies (in kcal mol^{-1}) and harmonic vibrational frequencies (in cm^{-1}) of the stationary points in the triplet state of the OH + HO_2 reaction system

			Frequencies								
Species	Note	E	1	2	3	4	5	6	7	8	9
OH + HO_2	PES[a]	0	3750		1138	1433	3656				
	Ab initio[b]	0	3738		1145	1439	3656				
	Ab initio[c]	0	3734		1160	1439	3645				
	Ab initio[d]	0									
	Expt.[e]	0	3738		1098	1392	3436				
CP1	PES[a]	−3.70	*i*151	*i*85	167	284	318	1159	1506	3490	3670
	Ab initio[b]	−3.25	170	221	306	462	523	1168	1526	3490	3644
	Ab initio[c]	−3.45	173	222	284	464	525	1183	1524	3482	3638
	Ab initio[d]	−8.0									
	Ab initio[f]	−3.21	164	213	286	468	513	1193	1548	3597	3709
O_2 + H_2O	PES[a]	−70.58	1603		1651	3831	3945				
	Ab initio[b]	−70.57	1605		1647	3832	3942				
	Ab initio[c]	−70.59	1608		1644	3831	3941				
	Ab initio[d]	−72.60									
	Expt.[e]	−70.96	1580		1595	3657	3756				
	Ab initio[f]	−70.85									
TS1	PES[a]	−1.45	*i*1044	*i*93	119	477	536	996	1475	1817	3726
	Ab initio[b]	−1.60	*i*730	*i*72	193	462	1021	1080	1465	2092	3715
	Ab initio[c]	−1.96	*i*658	101	209	463	840	1106	1486	2198	3715
	Ab initio[d]	0.50									
	Ab initio[f]	−2.38	*i*2105	104	212	477	663	1146	1469	1543	3775
TS2	PES[a]	23.05	*i*868	263	313	359	576	1035	1189	3713	3762
	Ab initio[b]	22.64	*i*922	301	318	411	597	1017	1133	3740	3747
	Ab initio[c]	22.40	*i*833	316	376	417	594	1023	1145	3741	3744
TS2a	PES[a]	23.46	*i*905	193	346	396	572	1074	1124	3785	3805
	Ab initio[b]	23.29	*i*977	264	346	452	608	1040	1123	3730	3744
	Ab initio[c]	23.13	*i*976	266	322	444	592	1027	1126	3725	3739

[a] This work, PIP-NN PES. [b] This work, CCSD(T)-F12a/AVTZ. [c] This work, CCSD(T)-F12a/AVDZ. [d] CCSD(T)/AVTZ//CCSD(T)/6-311G(d,p).[25] [e] See http://cccbdb.nist.gov/ and ATcT.[64,65] [f] W3X-L//CCSD/VTZ.[20]

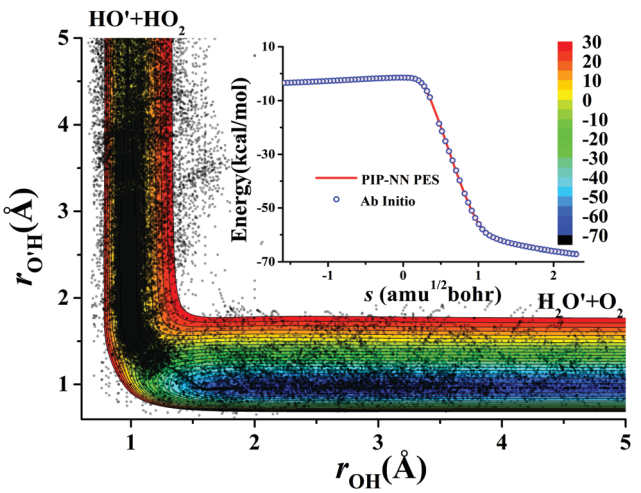

Fig. 4 Contour plot of the PES (energy in kcal mol^{-1}) for R1 as a function of the two reactive bond lengths. All other coordinates are fixed at TS1. The sampled points with the two reactive bond lengths up to 5 Å are also shown. The inset plot shows the corresponding minimum energy path on the PIP-NN PES and determined directly by *ab initio* calculation.

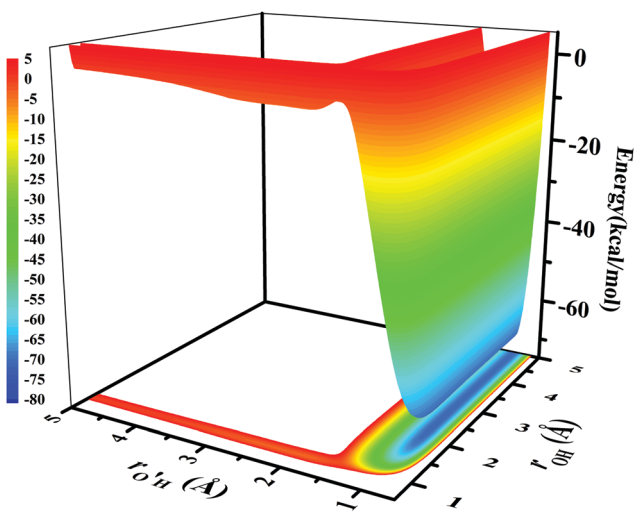

Fig. 5 Three-dimensional plot of the PES (energy in kcal mol^{-1}) for the O′H + HO_2 → H_2O' + O_2 channel as a function of the two reactive bond lengths with the other coordinates relaxed. The two-dimensional contour plot is also shown.

the product side are equivalent to each other, and the corresponding transition state possesses equivalent forming and breaking bonds. The PES is available from the corresponding authors upon request.

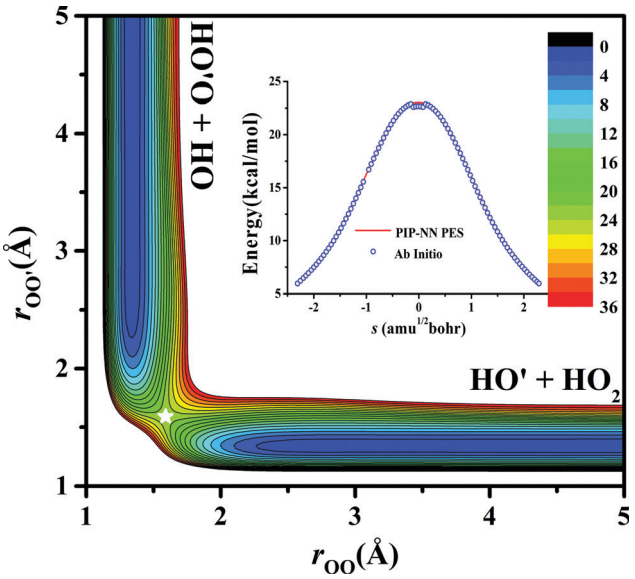

Fig. 6 Contour plot of the PES (energy in kcal mol^{-1}) for the OH + HO_2 → HO_2 + OH channel as a function of the two reactive bond lengths. All other coordinates are fixed at TS2. The inset plot shows the corresponding minimum energy path on the PIP-NN PES and determined directly by *ab initio* calculation.

III-C. Rate coefficients

Available experimental and theoretical rate coefficients of R1 are summarized in Fig. 7.[2,4–8,11,13,15–22,24–42] It can be seen that in the entire temperature range 300–2500 K, large differences, up to almost an order of magnitude, exist among different observations. Even in the same experiment, the results have large errors, due to the difficulty in measuring this radical–radical reaction. For instance, the observed data were quite scattered in the experiments by Kappel *et al.*[42] and by Srinivasan *et al.*,[18] within small temperature ranges. It is worth noting that there are no available experimental measurements at temperatures between 500 and 1000 K.

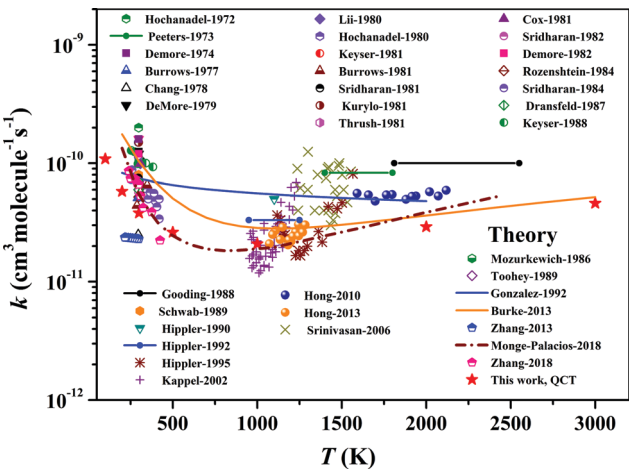

Fig. 7 Comparison of the thermal rate coefficients for the reaction OH + HO_2 → H_2O + O_2. The experimental error bounds are not included for clarity.

Theoretically, the computed results according to the vibrationally/rotationally adiabatic theory with MP4 predicted slightly negative temperature dependence in the range 200–2000 K.[24] Their data agree well with the measured values by Hong *et al.* in 1600–2200 K,[13] but significant deviations exist at temperatures 500–1200 K. Based on a detailed analysis of the existing results and *ab initio* calculations at the level of MS-CASPT2/CBS//MS-CASPT2/AVTZ, Burke *et al.* provided a quantitative explanation for the anomalous temperature dependence of the title reaction, and predicted a minimum in the rate coefficients near 1125 K.[16] As shown in Fig. 7, the temperature dependence is more remarkable at lower temperatures than at higher temperatures, as expected for a barrierless reaction. Recently, Monge-Palacios and Sarathy revisited the kinetics by using microcanonical and multistructural canonical transition state theories with the stationary information calculated at the level of W3X-L//CCSD(FC)/VTZ.[20] Their predicted rate coefficients also show a minimum, but at 850 K. On the other hand, the temperature dependence is also more significant than that predicted by Burke *et al.*[16] in the whole temperature range studied. In these transition-state-theory based approaches, only the information of the stationary points, such as the reactants, intermediates, and transition states, and minimum energy path, is required. Therefore, it is a very efficient means for providing a reliable estimation of the reaction rate coefficient. However, several assumptions or approximations are generally adopted. For instance, the vibration motions are generally treated as harmonic oscillators, and the tunneling contributions along the reaction coordinate are estimated according to the Eckart or Wigner model. In addition, it assumes that the reactants are at local equilibrium, and once the reactions reach the bottleneck, they proceed to products without ever returning. A relevant review is available.[66]

In this work, the QCT approach has been employed to calculate the rate coefficients of R1 at 100, 200, 300, 500, 1000, 2000, and 3000 K, and the results are also included in Fig. 6. It can be seen that QCT rate coefficients show a minimum at 1000 K. In addition, our QCT results are in better agreement with those by Monge-Palacios and Sarathy[20] at low temperatures, and with those by Burke *et al.*[16] at high temperatures. We conclude that the QCT results are in reasonably agreement with the experiment and theory, both of which are quite scattered.

Unlike the transition-state-theory based methods, QCT requires a full-dimensional PES, which covers all dynamically accessible regions of the reaction. Given an accurate PES, QCT can provide reliable rate coefficients if quantum effects are negligible. However, it cannot account for quantum mechanical effects, such as zero point vibrational energy, tunneling, *etc.* Therefore, some may think that the QCT rate coefficients at low temperatures might be underestimated. However, the R1 reaction is barrierless on the ground triplet electronic state. Therefore, the tunneling effect might be negligible for the R1 reaction. In the near future, we plan to employ more accurate treatments such as quantum scattering and ring-polymer molecular dynamics calculations on the PIP-NN PES to examine

these effects and their impacts on the reaction rate, which are beyond the scope of the current work.

IV. Summary and conclusions

In this work, we carry out theoretical studies on the kinetics of the prototypical radical–radical reaction $OH + HO_2 \rightarrow H_2O + O_2$ by the QCT approach. In particular, a globally accurate full-dimensional potential energy surface of the ground triplet state of the reaction is developed firstly based on 108 000 points calculated at the level CCSD(T)-F12a/AVTZ with careful treatment of the initial guess in the preceding Hartree–Fock procedure. QCT predicts a rate minimum at 1000 K, consistent with recent experiments. In addition, the QCT rate coefficients exhibit a remarkable negative temperature dependence at low temperatures, and a slight positive temperature dependence at high temperatures, again consistent with experiments. It is our hope that the current work can stimulate relevant experimental and theoretical efforts on the title reaction, which is important in interstellar, atmospheric, and combustion environments.

Conflicts of interest

There are no conflicts of interest to declare.

Acknowledgements

This work was financially supported by National Natural Science Foundation of China (Contract No. 21573027 to J. L.). H. S. acknowledges the support from National Natural Science Foundation of China (Contract No. 21603266). D. X. is thankful for financial support from the National Natural Science Foundation of China (Grant No. 21590802 and 21733006).

References

1 D. E. Heard and M. J. Pilling, *Chem. Rev.*, 2003, **103**, 5163–5198.
2 J. P. Burrows, G. W. Harris and B. A. Thrush, *Nature*, 1977, **267**, 233–234.
3 F. Kaufman, *Annu. Rev. Phys. Chem.*, 1979, **30**, 411–442.
4 U. C. Sridharan, L. X. Qiu and F. Kaufman, *J. Phys. Chem.*, 1981, **85**, 3361–3363.
5 M. J. Kurylo, O. Klais and A. H. Laufer, *J. Phys. Chem.*, 1981, **85**, 3674–3678.
6 L. F. Keyser, *J. Phys. Chem.*, 1981, **85**, 3667–3673.
7 U. C. Sridharan, L. X. Qiu and F. Kaufman, *J. Phys. Chem.*, 1982, **86**, 4569–4574.
8 M. Mozurkewich, *J. Phys. Chem.*, 1986, **90**, 2216–2221.
9 R. Atkinson, D. L. Baulch, R. A. Cox, J. N. Crowley, R. F. Hampson, R. G. Hynes, M. E. Jenkins, M. J. Rossi and J. Troe, *Atmos. Chem. Phys.*, 2004, **4**, 1461.
10 D. Stone, L. K. Whalley and D. E. Heard, *Chem. Soc. Rev.*, 2012, **41**, 6348–6404.
11 J. Peeters and G. Mahnen, *Symp. Combust.*, 1973, **14**, 133–146.
12 D. L. Baulch, C. T. Bowman, C. J. Cobos, R. A. Cox, T. Just, J. A. Kerr, M. J. Pilling, D. Stocker, J. Troe, W. Tsang, R. W. Walker and J. Warnatz, *J. Phys. Chem. Ref. Data*, 2005, **34**, 757.
13 Z. Hong, S. S. Vasu, D. F. Davidson and R. K. Hanson, *J. Phys. Chem. A*, 2010, **114**, 5520–5525.
14 C. Gonzalez, J. Theisen, L. Zhu, H. B. Schlegel, W. L. Hase and E. W. Kaiser, *J. Phys. Chem.*, 1991, **95**, 6784–6792.
15 W. B. DeMore, *J. Phys. Chem.*, 1982, **86**, 121–126.
16 M. P. Burke, S. J. Klippenstein and L. B. Harding, *Proc. Combust. Inst.*, 2013, **34**, 547–555.
17 J. J. Schwab, W. H. Brune and J. G. Anderson, *J. Phys. Chem.*, 1989, **93**, 1030–1035.
18 N. K. Srinivasan, M.-C. Su, J. W. Sutherland, J. V. Michael and B. Ruscic, *J. Phys. Chem. A*, 2006, **110**, 6602–6607.
19 Z. Hong, K.-Y. Lam, R. Sur, S. Wang, D. F. Davidson and R. K. Hanson, *Proc. Combust. Inst.*, 2013, **34**, 565–571.
20 M. Monge-Palacios and S. M. Sarathy, *Phys. Chem. Chem. Phys.*, 2018, **20**, 4478–4489.
21 P. Dransfeld and H. G. Wagner, *Z. Naturforsch., A: Phys. Sci.*, 1987, **42**, 471–476.
22 L. F. Keyser, *J. Phys. Chem.*, 1988, **92**, 1193–1200.
23 M. P. Badenes, M. E. Tucceri and C. J. Cobos, *J. Phys. Chem. A*, 2017, **121**, 440–447.
24 C. Gonzalez, J. Theisen, H. B. Schlegel, W. L. Hase and E. W. Kaiser, *J. Phys. Chem.*, 1992, **96**, 1767–1774.
25 T. Zhang, W. Wang, C. Li, Y. Du and J. Lu, *RSC Adv.*, 2013, **3**, 7381–7391.
26 T. Zhang, X. Lan, Z. Qiao, R. Wang, X. Yu, Q. Xu, Z. Wang, L. Jin and Z. Wang, *Phys. Chem. Chem. Phys.*, 2018, **20**, 8152–8165.
27 D. W. Toohey and J. G. Anderson, *J. Phys. Chem.*, 1989, **93**, 1049–1058.
28 C. J. Hochanadel, J. A. Ghormley and P. J. Ogren, *J. Chem. Phys.*, 1972, **56**, 4426–4432.
29 W. B. DeMore and E. Tschuikow-Roux, *J. Phys. Chem.*, 1974, **78**, 1447–1451.
30 J. S. Chang and F. Kaufman, *J. Phys. Chem.*, 1978, **82**, 1683–1687.
31 W. B. DeMore, *J. Phys. Chem.*, 1979, **83**, 1113–1118.
32 R.-R. Lii, R. A. Gorse, M. C. Sauer and S. Gordon, *J. Phys. Chem.*, 1980, **84**, 819–821.
33 C. J. Hochanadel, T. J. Sworski and P. J. Ogren, *J. Phys. Chem.*, 1980, **84**, 3274–3277.
34 B. A. Thrush and J. P. T. Wilkinson, *Chem. Phys. Lett.*, 1981, **81**, 1–3.
35 R. A. Cox, J. P. Burrows and T. J. Wallington, *Chem. Phys. Lett.*, 1981, **84**, 217–221.
36 J. P. Burrows, R. A. Cox and R. G. Derwent, *J. Photochem.*, 1981, **16**, 147–168.
37 V. B. Rozenshtein, Y. M. Gershenzon, S. D. Il'in and O. P. Kishkovitch, *Chem. Phys. Lett.*, 1984, **112**, 473–478.
38 U. C. Sridharan, L. X. Qiu and F. Kaufman, *J. Phys. Chem.*, 1984, **88**, 1281–1282.

39 J. M. Goodings and A. N. Hayhurst, *J. Chem. Soc., Faraday Trans. 2*, 1988, **84**, 745–762.
40 H. Hippler, J. Troe and J. Willner, *J. Chem. Phys.*, 1990, **93**, 1755–1760.
41 H. Hippler and J. Troe, *Chem. Phys. Lett.*, 1992, **192**, 333–337.
42 C. Kappel, K. Luther and J. Troe, *Phys. Chem. Chem. Phys.*, 2002, **4**, 4392–4398.
43 H. Hippler, H. Neunaber and J. Troe, *J. Chem. Phys.*, 1995, **103**, 3510–3516.
44 C. F. Jackels and D. H. Phillips, *J. Chem. Phys.*, 1986, **84**, 5013–5024.
45 T. B. Adler, G. Knizia and H.-J. Werner, *J. Chem. Phys.*, 2007, **127**, 221106.
46 G. Knizia, T. B. Adler and H.-J. Werner, *J. Chem. Phys.*, 2009, **130**, 054104.
47 B. Jiang and H. Guo, *J. Chem. Phys.*, 2013, **139**, 054112.
48 J. Li, B. Jiang and H. Guo, *J. Chem. Phys.*, 2013, **139**, 204103.
49 B. Jiang, J. Li and H. Guo, *Int. Rev. Phys. Chem.*, 2016, **35**, 479–506.
50 J. Li, S. Carter, J. M. Bowman, R. Dawes, D. Q. Xie and H. Guo, *J. Phys. Chem. Lett.*, 2014, **5**, 2364–2369.
51 M. Bai, D. Lu and J. Li, *Phys. Chem. Chem. Phys.*, 2017, **19**, 17718–17725.
52 D. Lu, C. Xie, J. Li and H. Guo, *Chin. J. Chem. Phys.*, 2019, **32**, 84–88.
53 H.-J. Werner, P. J. Knowles, G. Knizia, F. R. Manby, M. Schütz, *et al.*, *MOLPRO, version 2012.1, a package of ab initio programs*, see http://www.molpro.net.
54 M. L. Weichman, J. A. DeVine, M. C. Babin, J. Li, L. Guo, J. Ma, H. Guo and D. M. Neumark, *Nat. Chem.*, 2017, **9**, 950–955.
55 J. Li, C. Xie and H. Guo, *Phys. Chem. Chem. Phys.*, 2017, **19**, 23280–23288.
56 J. Li, K. Song and J. Behler, *Phys. Chem. Chem. Phys.*, 2019, **21**, 9672–9682.
57 Z. Xie and J. M. Bowman, *J. Chem. Theory Comput.*, 2010, **6**, 26–34.
58 J. M. Bowman, G. Czakó and B. Fu, *Phys. Chem. Chem. Phys.*, 2011, **13**, 8094–8111.
59 C. Qu, Q. Yu and J. M. Bowman, *Annu. Rev. Phys. Chem.*, 2018, **69**, 151–175.
60 L. M. Raff, R. Komanduri, M. Hagan and S. T. S. Bukkapatnam, *Neural Networks in Chemical Reaction Dynamics*, Oxford University Press, Oxford, 2012.
61 X. Hu, W. L. Hase and T. Pirraglia, *J. Comput. Chem.*, 1991, **12**, 1014–1024.
62 C. N. R. Rao, G. V. Kulkarni, A. M. Rao and U. C. Singh, *THEOCHEM*, 1984, **108**, 113–119.
63 C. F. Jackels, *J. Chem. Phys.*, 1993, **99**, 5768–5779.
64 B. Ruscic, R. E. Pinzon, M. L. Morton, G. von Laszevski, S. J. Bittner, S. G. Nijsure, K. A. Amin, M. Minkoff and A. F. Wagner, *J. Phys. Chem. A*, 2004, **108**, 9979–9997.
65 B. Ruscic, R. E. Pinzon, G. von Laszevski, D. Kodeboyina, A. Burcat, D. Leahy, D. Montoya and A. F. Wagner, *J. Phys.: Conf. Ser.*, 2005, **16**, 561–570.
66 A. Fernandez-Ramos, J. A. Miller, S. J. Klippenstein and D. G. Truhlar, *Chem. Rev.*, 2006, **106**, 4518–4584.